Green Chemistry

Accepted Manuscript

ROYAL SOCIETY OF CHEMISTRY

www.rsc.org/greenchem

Effect of Preparation Methods on the Performance of Co/Al_2O_3 Catalysts for Dry Reforming of Methane

Jessica L. Ewbank,[1,2] Libor Kovarik,[3] Christian Kenvin[1], Carsten Sievers[1,2*]

[1] School of Chemical & Biomolecular Engineering, Georgia Institute of Technology, Atlanta, GA 30032

[2] Institute of Paper Science, Georgia Institute of Technology, Atlanta, GA 30032

[3] Pacific Northwest National Laboratory, Environmental Molecular Sciences Laboratory, Richland, WA 99352

Abstract

Two methods, dry impregnation (DI) and controlled adsorption (CA), are used for the preparation of Co/Al_2O_3 catalysts for methane dry reforming reactions. Point of zero charge (PZC) measurements, pH-precipitation studies, and adsorption isotherms are used to develop a synthesis procedure in which deposition of Co^{2+} takes place in a more controlled manner than metal deposition during drying in synthesis by dry impregnation. The possible adsorption phenomena that occur during preparation of Co/Al_2O_3 catalyst by controlled adsorption are discussed. H_2 chemisorption and TEM show that catalysts prepared by CA have smaller average particle sizes and higher dispersions. TPR studies show that for the sample by CA a higher amount of cobalt is reduced to its metallic state and that more $CoAl_2O_4$ spinel species are present relative to DI samples. The catalyst prepared by CA shows higher activity and slower deactivation for methane dry reforming than the catalyst prepared by DI. XPS and C,H,N analysis on spent catalysts confirm two types of carbonaceous deposits are formed depending on the preparation method.

Introduction

Renewable energy sources are of growing importance and gasification of second generation biomass feedstocks is an attractive route for production of green fuels and chemicals. However, efficient cleaning and conditioning of biomass derived syngas is still a major technical barrier. [1] Biomass derived syngas generally has a high content of carbon dioxide and methane that must be either separated or reformed to CO and H_2 before the syngas is suitable for downstream processing to fuels or chemicals. Carbon dioxide separation is known to be expensive and thus, methane dry reforming is a desired step in upgrading of biomass derived syngas. [2] Dry reforming of methane has also attracted much attention due to increased interest in the effective utilization of these greenhouse gases. [2, 3]

Cobalt catalysts supported on γ-Al_2O_3 are commonly used for hydrogenation reactions, Fischer-Tropsch synthesis, [4] and hydrotreating of crude oil. [5] Cobalt catalysts have also found application as sulfur resistant catalysts and have been used for the WGS reaction. [6] However, few studies have focused on the use of cobalt catalysts for methane steam and dry reforming reactions. [7, 8]

Catalysts used in the investigation of methane dry reforming are commonly prepared using impregnation methods. Impregnation methods are routinely implemented to synthesize catalysts on an industrial scale. In dry impregnation (DI), a solution of metal salt is prepared in a volume of water sufficient to fill the pore volume of the support. [9] Often, in this method of preparation, only low weight loadings can be achieved because the concentration of the metal salt is beyond the solubility limit and successive impregnations must be carried out to achieve the desired weight loading. [10] One advantage of this method is that no filtration is necessary, and no metal is lost. However, the deposition of the metal precursor occurs through precipitation during drying.

[11] Thus, the resulting metal support interactions are very weak, and there is little control over the deposition of the metal often resulting in low dispersion. [9, 12]

In many studies, different results are obtained for similar catalytic systems because synthetic methods do not commonly exercise control of active site formation. [13] There has been much effort devoted to the fundamentals of catalyst synthesis so that the deposition of the metal precursor is controlled and catalysts can be synthesized in a reproducible manner. Strong electrostatic adsorption (SEA) is one such rational synthesis method that has been proven to be reproducible and results in catalysts with higher dispersions and smaller metal particles than catalysts prepared by impregnation methods. [6, 12, 14-21] Deposition of metal particles by SEA involves only electrostatic (non-specific) interactions between the metal precursor and the support. Some metal-support systems exhibit chemical (specific) interactions with the support in addition to electrostatic ones. Another rational synthesis method where the adsorption of the metal is controlled is equilibrium deposition filtration (EDF). Extensive work has been conducted on EDF preparation of catalysts where deposition of metal particles occurs through specific (in addition to non-specific) interactions such as adsorption through hydrogen bonds, formation of innersphere complexes, or interfacial precipitation. [11, 22-28] The extent to which any of the aforementioned types of specific interactions occurs depends on the nature of the complex, the ionic strength, and the impregnating temperature and time used during synthesis. [28]

The details of adsorption phenomena of metal precursors at the solid aqueous interface have long been, and are still, a source of disagreement. [22, 23, 25, 29-32] A non-specific interacting complex is weakly linked through electrostatic forces, van der Waals forces, or hydrogen bonding (e.g. SEA). Non-specific complexes can be accurately described using a double layer model in which only the outer Helmholtz plane (OHP) is considered (Figure 1a). [25] Specific interactions of a

metal complex with an oxide support can be described in terms of hydrogen bonds, ion pairing, or ligand exchange (e.g. EDF). To describe specifically interacting complexes a complex triple layer model is implemented where the OHP and inner Helmholtz plane (IHP) are considered (Figure 1b – 1d). The word "specific" indicates that adsorption constants differ within a group of cations of the same valence, an implication of this specificity is that not only electrostatic but also chemical interactions are involved in the adsorption process. [33] As noted by Haworth in his review of modeling sorption from aqueous solution it is difficult to distinguish between the effects of electrostatic and chemical interactions with oxide supports. [34]

In this paper, the possible adsorption phenomena that occur during catalyst preparation, the effect of preparation method on types of active sites formed, and catalytic activity of 2 wt% Co/Al_2O_3 in methane dry reforming reactions are explored.

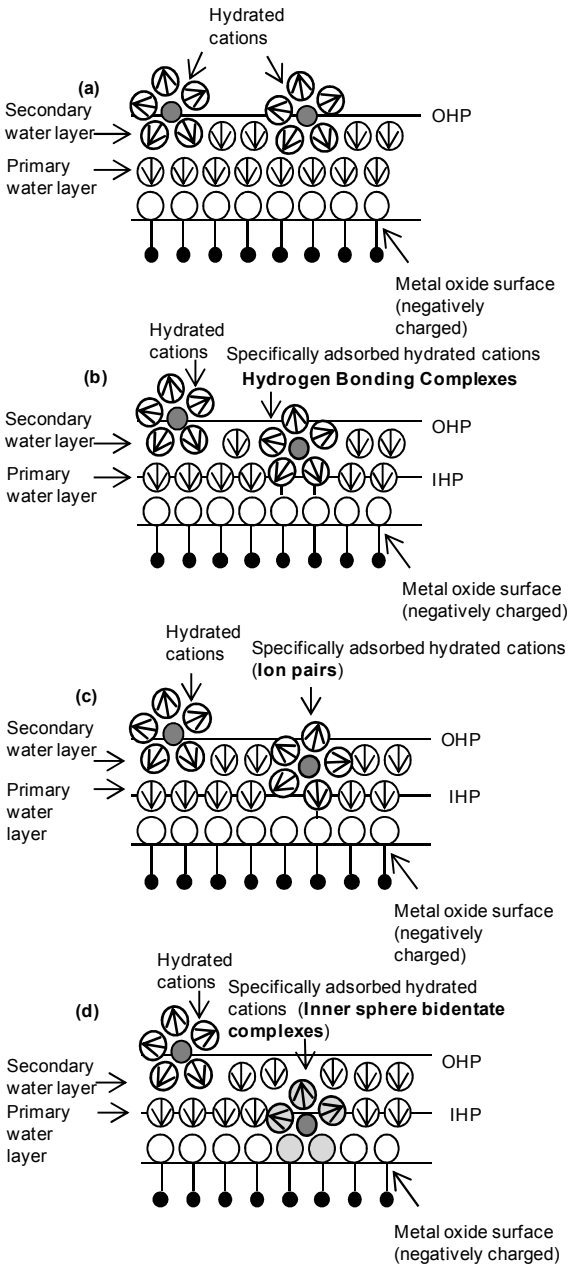

Figure 1 - (a) Non-specific (electrostatic) adsorption. Double layer description of the metal oxide-water interface where OHP is the outer Helmholtz plane. Specific adsorption of metal complexes at the oxide-water interface, best described using triple layer model where IHP is the inner Helmholtz plane. Complexes can specifically interact with the surface in

several ways, such as, (b) hydrogen bonding complexes (c) ion pairing (d) inner-sphere complexes. Based on [25].

Experimental

Materials

Aluminum oxide, γ-phase, 99.97% metals basis (Alpha Aesar, surface area 80 – 120m^2/g) was used as received. $Co(NO_3)_2$ (99.999% trace metals basis) from Aldrich was used as the metal precursor for catalyst synthesis. HCl and NaOH (A.C.S. reagent grade) from Sigma were used as pH adjustors in pH precipitation studies, adsorption isotherms, and catalyst synthesis as discussed below. Deionized water was used throughout this study.

Controlled Adsorption (CA) synthesis optimization

Point of zero charge

To determine the point of zero charge (PZC) of the γ–Al_2O_3 support, pH solutions ranging from 0.5 to 13 were prepared using HCl or NaOH. The mass of alumina used corresponded to a surface loading (S.L.) of alumina of 1000 m^2/L. The support was contacted with the solutions, shaken for one hour, and the final pH was then measured. A glass bodied Thermo Scientific Orion pH probe (9102BNWP) was employed for all pH measurements. The pH meter was calibrated using standard buffer solutions at the start of every experiment. The experiments were conducted using 50 mL polypropylene bottles at room temperature

pH precipitation studies

Solutions with pH values ranging from 5.5 to 13 were prepared using NaOH at room temperature. 200 ppm cobalt (as cobalt nitrate hexahydrate) was added to the solutions. The solutions were shaken for one hour, and the final pH was determined. Any sign of precipitation

(and its color) at a given pH value was noted. Solutions were then filtered using 0.2 μm nylon membrane filters.

Precursor adsorption as a function of time (constant pH)

200 ppm of cobalt (as $Co(NO_3)_2$) was added to an aqueous solution adjusted to a pH of 8.5 using NaOH at room temperature. Samples of the impregnating solution were taken at 30 minute intervals, and the pH re-adjusted to 8.5 for a total time of 2.5 hours. The liquid samples were filtered using 45μm nylon syringe filters and analyzed by ICP-OES using a Perkin Elmer Optima 3000 DV.

Catalyst Preparation

Controlled Adsorption (CA)

Cobalt was deposited using a cyclic procedure as described above. Specifically, 200 ppm of cobalt (as $Co(NO_3)_2$) was added to an aqueous solution adjusted to a pH of 8.5 using NaOH at room temperature. The pH of the impregnating solution was re-adjusted to 8.5 every 30 minutes using NaOH over a period of 2 hours at which time deposition of all cobalt in solution had occurred. The catalyst was then filtered and washed twice with deionized water. The 2 wt% Co/Al_2O_3 catalysts prepared in this cyclic manner will henceforth be designated 2CoCA (controlled adsorption).

Dry Impregnation (DI)

The weight loading for catalysts prepared by dry impregnation was chosen to be the same as the 2CoCA catalyst. The desired amount of complex was dissolved in a volume of water that corresponded to the pore volume of the support as determined by nitrogen physisorption. The precursor solution was added to the support and allowed to stir for 1 h at room temperature. The 2 wt% Co/Al_2O_3 catalysts prepared in this manner will henceforth be designated 2CoDI.

Calcination

Prepared catalysts were dried in an oven at 110 °C for 10 minutes prior to calcination. Samples prepared by different methods were heated to 500 °C. Zero air generated using a zero air generator (VWR, 26000-020) at a flowrate of 150 mL/min and a heating rate of 5 °C/min. The zero air generator produces UHP zero air with a purity level below 0.05 ppm total hydrocarbon content from the compressed air supply. Samples were calcined for 3 h.

Characterization

Nitrogen Physisorption

N_2 adsorption/desorption isotherms at -196 °C were measured for calcined catalysts using Micromeritics ASAP 2020. Approximately 0.5 g of sample was used in all experiments to minimize instrument error. The samples were outgassed for 3 h under vacuum at 300 °C. The specific surface area was calculated using the BET equation.

Elemental Analysis

To determine the cobalt content, the 2CoDI and 2CoCA catalysts were externally analyzed for cobalt and aluminum concentration by Gailbraith laboratories. HF digestion was used to dissolve the alumina support so that the cobalt content could be accurately determined by ICP-OES.

Temperature-programmed reduction

Temperature programmed reduction was carried out using Micromeritics ASAP 2920 equipped with a TCD detector, a reference chamber, and a cold trap. The cold trap contained a mixture of dry ice and isopropyl alcohol. The reducing gas was a 10% H_2/Ar mixture at a gas flowrate of 50 mL/min, and approximately 40 mg of catalyst was used in all experiments. The temperature was ramped from 25 °C to 1000 °C at 5 °C/min. Obtained traces were normalized with respect to the amount of sample used during the experiment.

H_2 Chemisorption

Metal dispersion was analyzed using a Micromeritics Chemisorb 2750 using hydrogen. The sample was evacuated at 110 °C for 60 min to remove ambient gases. The temperature was ramped from 110 °C to 600 °C at 2 °C/min and held at 600 °C for 8 h. The sample was then evacuated and cooled to 550 °C and held there for 16 h to remove residual hydrogen. Finally, the sample was cooled to 25 °C at which time H_2 gas was dosed and the analysis was performed. Two isotherm measurements were performed and the metal surface area was calculated using H/M ratio of 1. [35] Approximately 40 mg of catalyst was used in all experiments.

Transmission Electron Microscopy

Transmission electron microscopy (TEM) observations were performed with a FEI Titan 80-300 operated at 300 kV. The instrument is equipped with CEOS GmbH double-hexapole aberration corrector for image-forming lens, which allows imaging with sub angstrom resolution. Compositional analysis was performed with EDAX Si(Li) EDS detector, and the analysis of the obtained spectra was performed with FEI TIA software. The samples for TEM observations were prepared by dispersing a dry powder on a lacey-carbon coated 200 mesh Cu TEM grids. The as prepared grids were then immediately loaded into the TEM airlock to minimize an exposure to atmospheric O_2.

X-ray Photoelectron spectroscopy

XPS was performed on post reaction catalysts using a Thermo K-Alpa instrument equipped with a monochromatic small-spot X-ray source and a 180° double focusing hemispherical analyzer with a 128-channel detector. Spectra were obtained using an aluminum anode Al Kα ($h\nu$ = 1486.6 eV). The background pressure was 4.9×10^{-8} bar and 4×10^{-7} bar argon during measurement because of the charge compensation dual beam source which was used to prevent

sample charging. The binding energies were referenced to the sample stage which contains built in calibration standards of copper, silver, and gold.

Reactivity studies

Methane dry reforming reactions were performed in a quartz reactor using a stoichiometric mixture of methane and carbon dioxide. Reactivity studies were conducted using 200 mg of catalyst. Catalyst samples were reduced in-situ at 600 °C in a 20% H_2/N_2 mixture for two hours prior to reactivity studies. A space velocity of 22,000 h^{-1} of reactant gas was employed. The temperature was 700 °C and pressure was atmospheric. Product gas was sampled at 20 minute intervals using an online Bruker 450-GC refinery gas analyzer (RGA). The RGA is equipped with two TCD detectors and a FID. One TCD is used for analysis of hydrogen and the second for analysis of permanent gas mixtures (including methane). The FID channel allows for identification of methane and higher hydrocarbons (and confirmation of methane concentration from the middle TCD). Spent catalysts were externally analyzed for C, H, N concentrations by Gailbraith laboratories to determine the amount of carbonaceous material deposited on used catalysts.

Results and Discussion

2CoCA synthesis optimization

Point of Zero Charge

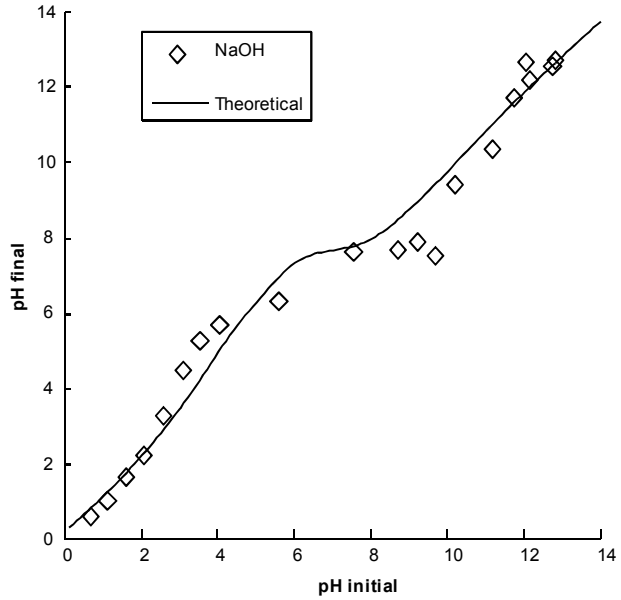

Figure 2 - Experimental PZC data fit with theoretical model. Adjustable parameters, PZC = 7.7. Adjustable theoretical model parameters; difference between pK_1 and pK_2 (ΔpK) = 5.0, Number of charged sites (N_S) = 8 OH/nm^2, [36] 25 °C.

The point of zero charge (PZC) of a metal oxide support is the point at which the support surface is neutrally charged. At pH values above the PZC of the metal oxide the surface is deprotonated (negatively charged) and cationic species can be electrostatically adsorbed. At pH values below the PZC the surface is protonated (positively charged) and anionic species can be adsorbed. The metal precursor used in this study ($Co(NO_3)_2$) is cationic. To define appropriate conditions for Co^{2+} deposition, it was necessary to determine the point of zero charge (PZC) of the alumina support. The plateau (Figure 2) represents the PZC and exists because the number of surface OH groups far outnumbers the quantity of OH^- ions initially present in solution. [12] Consequently, alumina buffers the solution at its PZC. The PZC of alumina used in our study was found to be at a pH of 7.7. The value of the PZC was determined by averaging the data points that comprise the plateau in Figure 2. Details of the theoretical model applied to the PZC data can be found in [36]. Briefly, two parameters of the model are adjustable; the total number of charged sites N_s and the

difference between pK_1 and pK_2 (ΔpK). For alumina, these values can be readily found in literature; N_s = 8 OH/nm^2 and ΔpK = 5. [29, 37] It should be noted here that, ideally, to adsorb cations by a purely electrostatic mechanism a support with a lower PZC is selected. [12] However, for reforming applications, low PZC materials such as silica or most amorphous silica alumina are not viable. Specifically, the high acidity of typical amorphous silica-alumina increases coking during catalytic reactions at high temperature. Coking is one of the main deactivation mechanism of methane dry reforming catalysts reported in literature. [8] Additionally, the high reaction temperature required for reforming reactions may cause vaporization of silica. [38] Therefore, alumina is a much more suitable support for the reaction conditions studied herein.

pH-precipitation studies of Co^{2+}

The PZC of the alumina used in this study is relatively high for adsorption of cationic complexes. Because the PZC of alumina is at a pH of 7.7, one must be concerned about partial dissolution of the support at high pH and also precipitation of cationic complexes in highly alkaline solutions. The use of cationic precursors of cobalt was desired to avoid the use of anionic cobalt complexes, which are often toxic, water insoluble, or large organic molecules [39] and thus undesirable for industrial application. To investigate cobalt cation complex stability in alkaline solutions, the desired concentration of $Co(NO_3)_2$ was added to solutions with pH values between 5.5 and 13. The first point at pH of 5.5 corresponds to pure deionized water with no base added. Initial pH refers to the pH of the solution without $Co(NO_3)_2$ and the final pH refers to the pH of the solution after contact with 200 ppm Co^{2+} for one hour. The resultant metal solutions were subsequently filtered and the color of precipitate was noted. The point of bulk precipitation observed upon filtering of the solutions is indicated by the line in Figure 3.

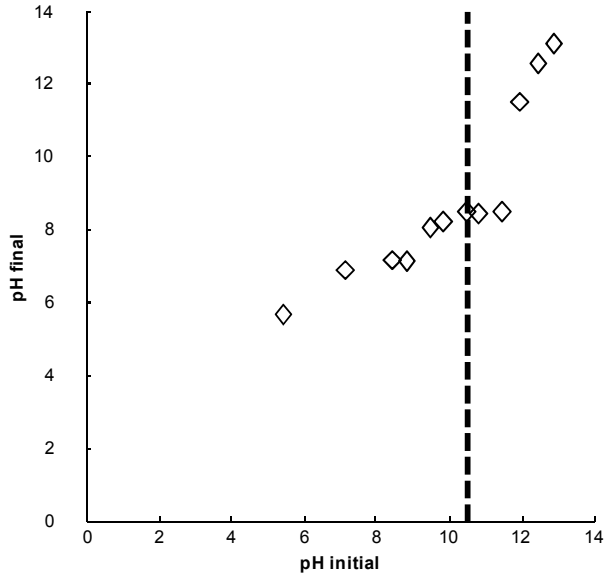

Figure 3- pH shift of Co^{2+} (as cobalt nitrate) in NaOH and point of observed precipitation (- - -), 25 °C.

The metal precursor solution shifted the pH of the mixture due to equilibration of the various types of ionic species in solution. As expected, Co^{2+} was found to have low solubility at alkaline conditions. The color of the precipitate was observed to change from blue to green to brown with increasing pH. The blue precipitate is indicative of unstable $Co(OH)_2$. [39] The green precipitate is thought to be formed by oxidation or mixing of various types of cobalt hydroxide (e.g. unstable/stable $Co(OH)_2$). The brown precipitate results from pale pink $Co(OH)_2$ that has been freshly precipitated with NaOH and oxidized to brown CoO(OH). [39] The various amounts and types of precipitation that occur at each pH point examined indicate complex solution chemistry. Several important synthesis considerations are revealed in light of this study: pH ranges where bulk precipitation occurs are identified and thus can be differentiated from adsorption during adsorption isotherm measurements (vide infra); the metal precursor should be allowed to equilibrate followed by re-adjustment of the mixture to the desired pH value before contact with

the support; the types of cobalt species that exist in solution are dependent on the pH value being examined. It should be noted that once alumina is added to the alkaline cobalt solution additional species could be formed in solution, however, valuable insight has been obtained regarding bulk solution behavior.

CA Adsorption Studies

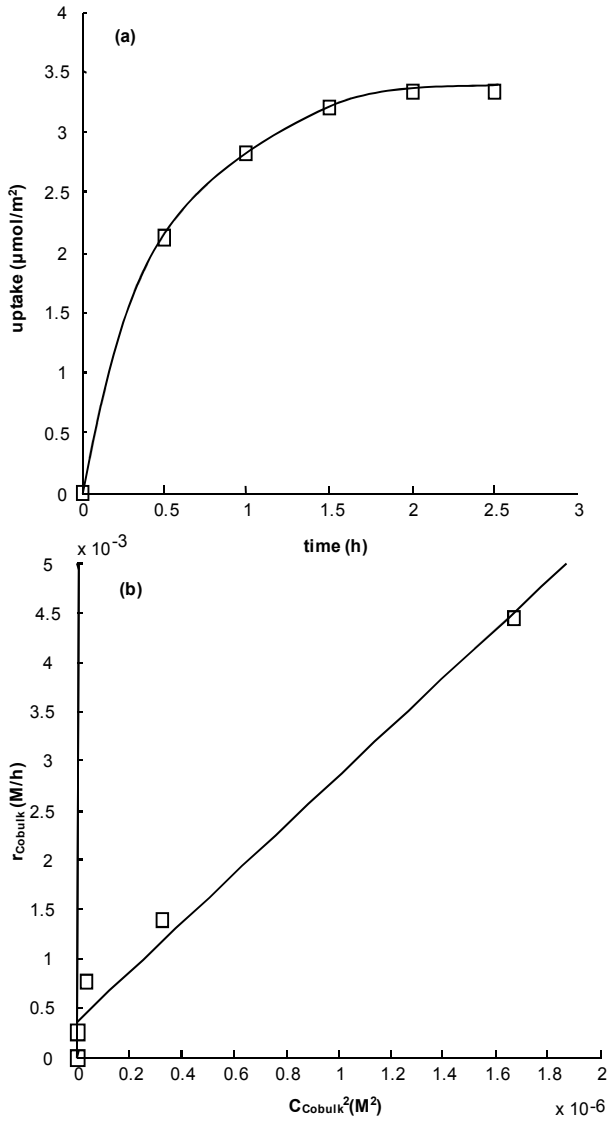

Figure 4 – (a) Experimental data for cyclic Co deposition at 25 °C (b) kinetic expression for $Co(II)(NO_3)_2$ deposition at C_{Cosurf} = 4.2 µmolm^{-2} (1 theoretical surface layer of $Co(H_2O)_6^{2+}$) [31, 36] , k' = 2573.5 (L mol^{-1} h^{-1}), R^2 = 0.978.

Figure 4a shows the experimental data for Co^{2+} uptake as a function of contact time with the support at a constant pH of 8.5. This pH was selected so that the pH of the impregnating mixture was above the PZC of the support and below pH values where bulk precipitation was observed. The pH of the impregnating solution was adjusted to a value of 8.5 every 30 minutes, similar to the approach of Lycourghiotis et al., [27] and a sample was taken to monitor the removal of cobalt from the impregnant solution. Deposition of all cobalt in solution was completed by 2 hours as shown in Figure 4a. In Figure 4b the rate of disappearance of cobalt from the bulk solution is plotted versus the square of the concentration of Co^{2+}. Following Lycourghiotis et. al., [27] cobalt deposition can be described by the kinetic equation,

$$r_{Co,bulk} = k'C^2_{Co,bulk} \quad (1)$$

The above kinetic expression was derived assuming the following deposition scheme,

$$nS + 2[Co(H_2O)_6]^{2+} \rightarrow S_n - [Co(H_2O)_{x,x<6}^{2+}]_2 \quad (2)$$

Where, S is a surface receptor site on the metal oxide support and n is the number of surface sites. This mechanism implies that two $Co(H_2O)_6^{2+}$ ions are adsorbed on a surface site, possibly due to simultaneous adsorption and dimerization of two interfacial cobalt ions through (hydr)oxo-bridges, and is depicted in Figure 5. However, such a synchronized event is rather unlikely to occur. We alternatively suggest that the rate of cobalt deposition is controlled by the dimerization of $[Co(H_2O)_6]^{2+}$. Once this has occurred adsorption of the dimer appears to be fast.

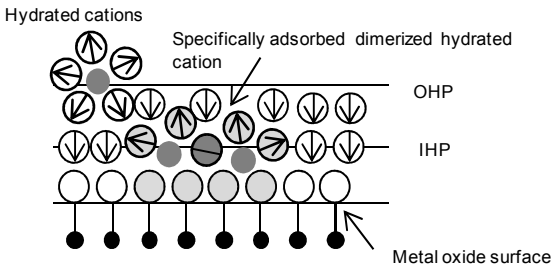

Figure 5 - Kinetic deposition of cobalt dimers at the alumina interface. $[Co(H_2O)_6]^{2+}$ dimerizes in solution and then is rapidly adsorbed onto the surface.

The kinetic equation (Equation 1) derived from a specific interaction deposition scheme suggested by Lycourghiotis et al. is sufficient to describe the adsorption phenomena in this study. [24] Since the pH used during adsorption isotherms (pH = 8.5) is close to the PZC of the support, it is likely that there is a low concentration of deprotonated surface hydroxyls. Thus, it is favorable for cobalt ions that are close to the surface dimerize because this reaction allows the cobalt species to bridge between two separated surface hydroxyls without increasing its charge. Once the dimers have formed, they rapidly adsorb. Additionally, non-negligible deposition near the PZC of the support is indicative of specific interactions. Co^{2+} deposition on alumina has been reported to exhibit mostly specific interactions and the nature of the metallic complex and its interaction(s) with the solid surface seem to play an important role. [24, 25, 32, 40] Extensive work has been conducted at the University of Patras on the application of equilibrium adsorption filtration (EDF) of Ni and Co on Al_2O_3. [11, 22-27] Lycourghiotis found that for Co(II) adsorption on alumina, above 0.33 theoretical $[Co(H_2O)_6]^{2+}$ layers the Co(II) speciation changes from binuclear, oligonuclear, and multinuclear inner-sphere surface complexes to $Co(OH)_2$ like precipitate at relative high Co(II) surface concentrations. It was found that these $Co(OH)_2$ precipitates formed at lower pHs than those required for bulk precipitation. [24] In this study, one theoretical

$[Co(H_2O)_6]^{2+}$ surface layer was used to minimize the amount of $Co(OH)_2$ precipitation while still preparing a catalyst with a reasonable cobalt content, e.g. 2 wt% cobalt-alumina. Another important implication of utilizing low weight loading cobalt on alumina catalysts is the idea that the dispersion can be increased thus decreasing coke formation since large particles stimulate coke formation. [41]

Characterization of 2wt% Co/Al_2O_3 catalysts prepared by CA and DI

N_2 physisorption, Elemental Analysis, H_2 chemisorption, and TEM

Table 1 shows the results from N_2 physisorption, elemental analysis, and H_2 chemisorption measurements. Elemental analysis confirmed that 2CoCA and 2CoDI had the desired amount of cobalt. The surface area was similar for catalysts prepared by both methods. The supported Co catalysts had slightly lower surface area and larger pore volume and pore diameter than that of the fresh alumina support presumably, due to phase transformation of the alumina support and precipitation of the metal precursors upon calcination. H_2 chemisorption measurements show that 2CoCA catalysts have a higher dispersion and smaller metal particle size than the 2CoDI sample. The reported values of dispersion are within the range of those reported for cobalt alumina catalysts in literature. [42-44]

Table 1 - N_2 physisorption, elemental analysis, and H_2 chemisorption of prepared catalysts.

Sample	Surface Area (m^2/g)[a]	Pore Volume (cm^3/g)[b]	Average Pore Diameter (nm)[c]	Elemental Analysis (wt% Co)[d]	Average Metal Particle Diameter (nm)[e]	Dispersion (%)[f]
2CoCA	**88**	**0.35**	**14.7**	**2.01**	**19.4**	**5.1**
2CoDI	**84**	**0.31**	**16.0**	**2.02**	**28.0**	**3.5**

Fresh Alumina	**91**	**0.24**	**10.8**	**-**	**-**	**-**

[a] Calculated from N_2 physisorption data using the BET equation

[b] Calculated from N_2 physisorption data using single point adsorption at $P/P_0 = 0.99$

[c] Calculated from N_2 physisorption data using 4V/A from BET

[d] Elemental analysis determined using ICP

[e] Average cobalt crystallite size calculated using H_2 chemisorption data

[f] Cobalt dispersion calculated using H_2 chemisorption data

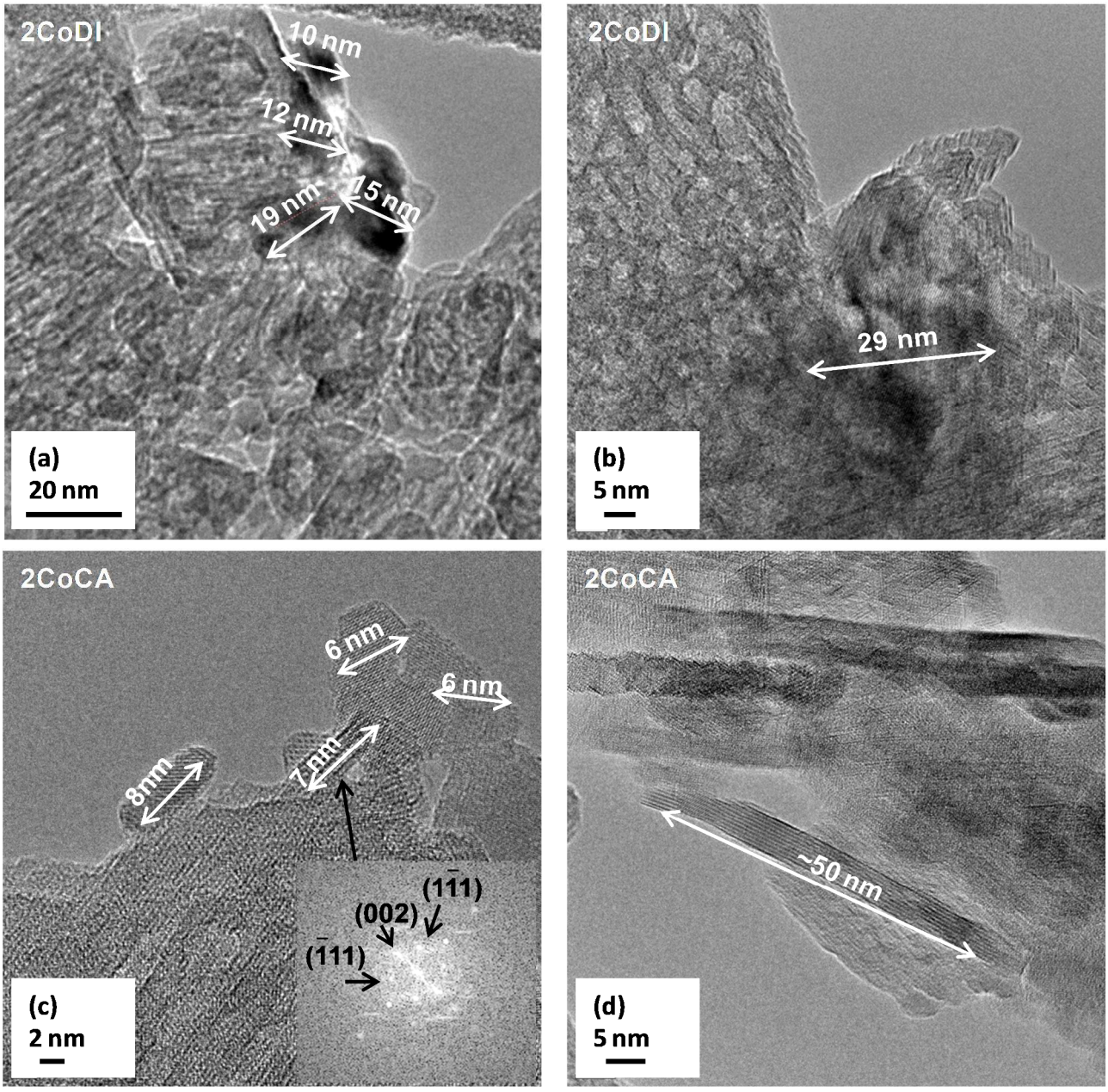

Figure 6 – Top: 2wt%Co/Al_2O_3 prepared by DI. Bottom: 2wt% Co/Al_2O_3 prepared by CA.

TEM images show that Co/Al_2O_3 prepared by DI contained Co particles that range from 10 to 40 nm in size (Figure 6a and b). In contrast, most Co particles on Co/Al_2O_3 prepared by CA were significantly smaller (*i.e.* 6-8 nm) as shown in Figure 6c and d. However, large particles are also present on the CA samples, which contribute to the average reported particle size by chemisorption (Figure 6d). As mentioned in the discussion of the synthesis of cobalt-alumina catalysts by CA, the deposition of Co^{2+} likely takes place through dimerization of cobalt ions and specific interactions with the alumina surface. Based on TEM images, it is speculated that in some instances, large oligomers are formed in solution and adsorbed on the surface or interfacial precipitation occurs leading to the observed large particles. Careful control of the mode of interfacial deposition could allow for a much finer tuning of the size of supported metal particles. [28] It is suggested that the formation of oligomers and the occurrence of surface precipitation could be avoided by reducing the initial concentration of cobalt in the impregnating mixture and performing successive impregnation steps with intermittent mild calcination treatments. This successive type impregnation to control the mode of deposition was successfully demonstrated for Pt/C catalysts prepared by strong electrostatic adsorption. [45] In the case of cobalt-alumina catalysts by DI, deposition of the Co^{2+} takes place during drying/calcination. Since this deposition method lacks the strong interaction with well-dispersed surface sites, the large average size of the particles is not surprising.

Temperature Programmed Reduction

Figure 7 shows the hydrogen concentration measured using a TCD detector during temperature programmed reduction (TPR) experiments for prepared catalysts, and Table 2 shows the hydrogen consumption normalized by the catalyst weight used in the experiment.

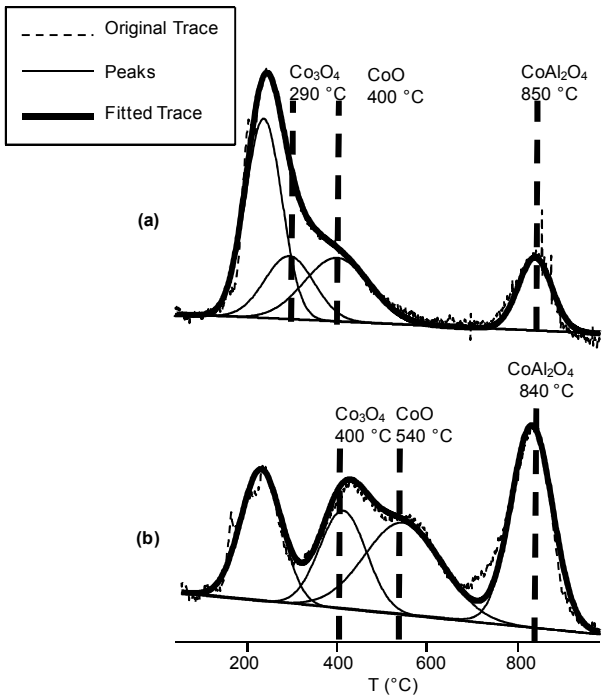

Figure 7 – TPR profiles (a) 2CoDI (b) 2CoCA

Table 2 – Hydrogen consumption per gram of sample for different TPR peaks based on TCD signal.

Peak Assignment	-NO_3 [a]	Co_3O_4 → CoO	CoO→ Co^0	$CoAl_2O_4$
2CoDI ($\mu molH_2/ g_{cat}$)	-	79	105	61
2CoCA ($\mu molH_2/ g_{cat}$)	-	93	141	168

[a] Hydrogen consumption omitted due to volatilization of nitrate species that affect TCD response

Four distinct peaks were observed during TPR experiments. The first peak at approximately 200 °C for both samples is attributed to decomposition of residual nitrate. [46, 47] The 2CoDI catalyst desorbs more residual components than the 2CoCA sample. This is expected because the 2CoCA sample was washed twice with de-ionized water prior to calcination. Due to the expected desorption of species other than H_2 (e.g. NO_2, NO, N_2O_5, NH_3, etc.) and their contribution to the

TCD signal, the exact values of H_2 consumption for the first peak are omitted. The total hydrogen consumption (excluding the first peak) corresponds to a total reduction from TPR of 60% for 2CoCA and 40% for 2CoDI. Peaks in the region of 300 °C and 600 °C are usually assigned to reduction of Co_3O_4 to CoO followed by CoO reduction to metallic Co. [48-50] In most TPR studies on supported Co catalysts, it is concluded that two phases exist on the support: a crystalline phase as Co_3O_4 and stoichiometric and non-stoichiometric cobalt aluminate. [44, 51, 52] Following literature assignments, the fourth peak in the TPR spectra is attributed to reduction of surface $CoAl_2O_4$.

For the reduction of Co_3O_4 to Co^0, the two reduction steps are not always observed as separate TPR peaks, [7, 44] as can be seen in Figure 7a. It has been found that strong interactions between the support and Co_3O_4 crystallites can manifest separation of the two reduction peaks, [44] as can be observed in Figure 7b. This is expected as the CA preparation method should cause stronger metal support interactions than DI. 2CoDI samples have peaks at 290 °C and 400 °C, whereas the corresponding CA prepared samples exhibit two very distinct peaks at 400 °C and 540 °C. The 100 °C separation between the two reduction peaks is commonly noted. [49] Additionally, 2CoCA samples have higher reduction temperatures than the corresponding DI sample, again, due to stronger metal support interactions induced by preparation method. It is possible that an additional peak exists at approximately 600 °C for the 2CoDI sample. This peak could be assigned to reduction of Co^{2+} to Co^0 where the Co^{2+} is surrounded by more Al^{3+}. [53] This would create a polarization of CoO bonds, and thus these cobalt particles would be more difficult to reduce (and appear at a higher temperature) than the large peak at 410 °C attributed to reduction of Co^{2+}. However, due to the small quantity of H_2 consumption it is assumed that this species, if it exists, is a minor component in the overall catalyst structure.

The areas of the two main peaks in the region of 300-700 °C are of great interest. From reduction stoichiometry, the ratio of the two peaks should be 1:3 for complete reduction. However, we see that for the 2CoDI sample a 1:1.3 ratio is obtained and for the 2CoCA sample a 1:1.5 ratio is obtained. Thus, the amount of cobalt reduced to its metallic state during TPR is greater in the 2CoCA sample than in the 2CoDI samples. Further, the obtained ratios indicate that neither of the samples is fully reduced to metallic state. Incomplete reduction of Co/Al_2O_3 catalysts is commonly cited in literature. [44, 54, 55] Guczi et al. reported a similar finding in his study of Pt-Co bimetallic catalysts. They concluded that the ratio of TPR peaks corresponding to Co_3O_4 to CoO and CoO to Co^0 was not 1:3 due to redisperison of the Co^{2+} ions spreading over the alumina, increasing the amount of Co surface spinel phase. [50, 53]

The fourth TPR peak, which is attributed to $CoAl_2O_4$ species, is much more pronounced in 2CoCA than 2CoDI samples. It seems reasonable that 2CoCA contains a greater amount of spinel phase because the preparation of this catalyst should cause strong metal support interaction and thus, surface spinel formation may be easier due to the intimate contact between the metal and support. It is currently not clear whether the cobalt spinel phase occurs during preparation, calcination, or reduction. However, from TPR, it can be observed that more reducible spinel species exist in the CA prepared catalysts and this catalyst visibly changes from dark green to light blue (indicative of $CoAl_2O_4$) after reduction/reaction, which could point to spinel formation during reduction. [56] Yan et al. found that the formation of $CoAl_2O_4$ occurred only after treatment at 800 °C. [54] This high temperature treatment was said to promote the dispersion of Co_3O_4 clusters and resulted in the formation of $CoAl_2O_4$. As discussed in the preceding paragraph, the redispersion of the cobalt during TPR might explain the observed non-stoichiometric reduction.

Catalytic Tests

Few studies have compared the activities of catalysts for carbon dioxide reforming of methane prepared by different methods and those only focused on different impregnation methods. [2, 3, 8, 57, 58] To test the activity of catalysts prepared by DI and CA, methane dry reforming experiments were conducted for 8 hours at 700 °C using a stoichiometric feed of carbon dioxide and methane. The desired reaction is, [43]

$$CH_4 + CO_2 \leftrightarrow 2CO + 2H_2 \quad \Delta H^0_{298K} = 247kJ/mol$$

The inverse water-gas shift reaction may impact the target reaction,

$$CO_2 + H_2 \leftrightarrow CO + H_2O \quad \Delta H^0_{298K} = 41kJ/mol$$

Steam generation from the above reaction could promote the methane steam reforming reaction,

$$CH_4 + H_2O \leftrightarrow CO + 3H_2 \quad \Delta H^0_{298K} = 206kJ/mol$$

However, one of the major drawbacks of methane dry reforming catalysts is their deactivation due to carbonaceous deposits,

$$CH_4 \rightarrow C + 2H_2 \quad \Delta H^0_{298K} = 75kJ/mol$$

$$2CO \rightarrow C + CO_2 \quad \Delta H^0_{298K} = -171kJ/mol$$

San Jose et al. found an initial conversion of methane of 75% for a 9 wt% Co/Al_2O_3 catalyst at 700 °C, SV 20,000 h^{-1}, and stoichiometric CH_4:CO_2. [2] Remarkably, this catalyst was also found to have the highest amount of carbon deposited. It was concluded that the large Co particles (~14 nm) produced non-deactivating carbon deposits and were involved in long term conversion. In a subsequent work, San Jose et al. studied Co/Al_2O_3 catalysts with low metal loading. Under similar conditions to those utilized in this work (2.5 wt% Co/Al_2O_3, 700 °C, SV= 20,000 h^{-1},

CH_4:CO_2 ratio 1:1), they found that the initial conversion of methane was about 35% and decreased by 12% over 6 h. [58] Zhang et al. studied methane dry reforming activity of bimetallic Ni-Co-Mg-Al-O co-precipitated catalysts. [43] Conversion of methane was stable over 28 h reactivity tests and H_2/CO yields of unity were reported. In many studies, the H_2/CO ratio is found to be less than unity due to the reverse water gas shift reaction. [8] Zhang et. al also found higher methane conversion activity for lower metal loadings of Ni-Co when compared to catalysts that had higher loadings. [43] The methane conversion, carbon dioxide conversion, and H_2/CO molar ratio achieved for prepared catalysts are illustrated in Figure 8.

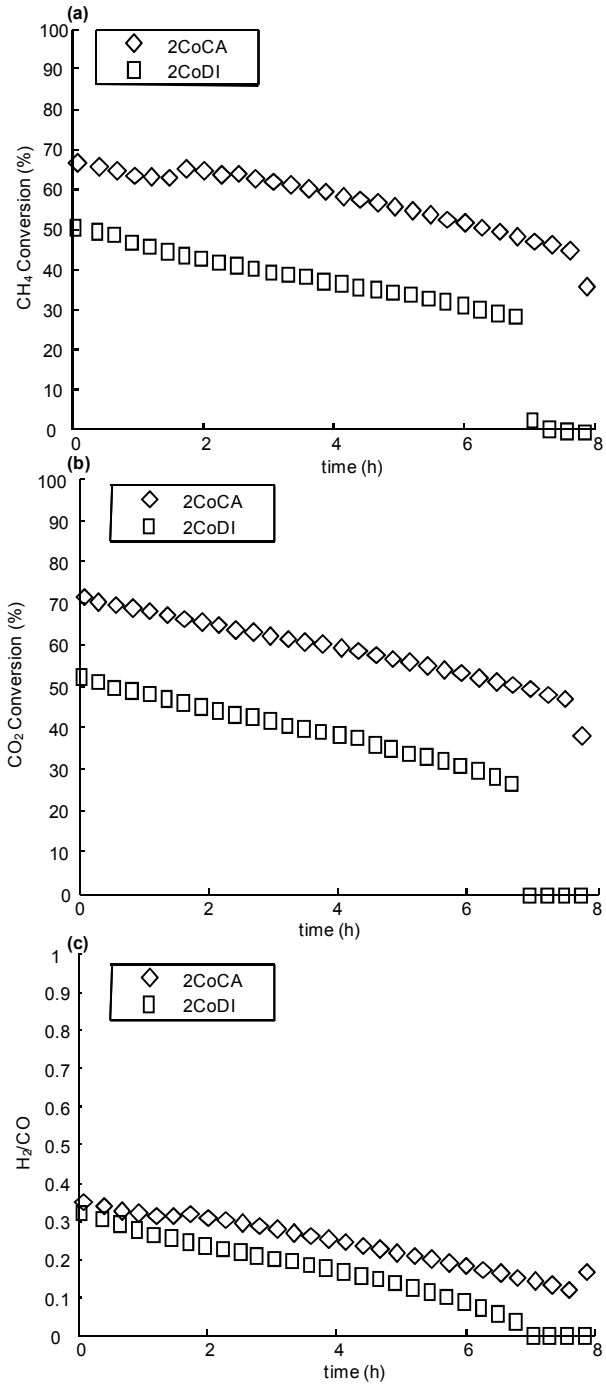

Figure 8 – (a) Methane conversion (b) Carbon Dioxide conversion (c) H_2/CO ratio for 2CoCA and 2CoDI at 700 °C and atmospheric pressure using a stoichiometric feed of carbon dioxide and methane.

2CoCA initially converted 68% of the methane and 71% of the carbon dioxide fed while 2CoDI catalysts initially converted 52% of each of the reactants fed. The H_2/CO ratio is initially 0.35 for 2CoCA and 0.33 for 2CoDI. Interestingly, due to the direct quantification of hydrogen, the H_2/CO ratio found in this study is lower than most other works where the H_2 concentration was estimated. [2, 43, 59] The high initial conversion indicates 2CoCA catalysts uses the Co present very effectively as these conversions are comparable to Co/Al_2O_3 catalysts with much higher weight loadings. [2] The difference appears to be due to the higher dispersion of Co in the 2CoCA sample. As noted earlier, the stability of cobalt alumina catalyst is of major concern. In this study, catalysts were only stable for the first two hours of reaction followed by slow but steady deactivation. In the context of methane dry reforming, there are three major possibilities for catalyst deactivation: sintering, metal oxidation and/or coking. Metal sintering might cause catalyst deactivation, however, the catalyst reduction temperature utilized prior to reactivity studies was quite high (600 °C, 2h). In a comparable study, Ferreira-Aparicio et al. showed that 5 wt% Co/Al_2O_3 did not deactivate due to sintering during methane dry reforming over a wide range of temperatures after calcination at 500 °C (3h) and reduction at 400 °C (4h). [60] Moreover, it is unlikely that the rapid deactivation after 7 hours on stream is caused by sintering, since sintering should deactivate the catalyst more steadily. Metal oxidation has been reported as a deactivation mechanism of cobalt based catalysts. [41, 43, 61, 62] The presence of oxygen from the dissociation of carbon dioxide can be responsible for the oxidation of cobalt under experimental conditions, [61] and thus the atmosphere on the surface may be both reducing and oxidizing. [41] Extrapolation of thermodynamic data for cobalt oxidation [63] indicates that cobalt oxidation is unlikely from the reaction conditions used in this study (low $p(H_2O)/p(H_2)$ ratio, high temperature). Due to the pronounced differences in the analysis of post reaction catalysts by

C,H,N and XPS, we suggest that coking is the dominant route of catalyst deactivation, in the present study.

The most common problem of methane dry reforming on a commercial scale is catalyst deactivation due to coking. [8] Catalysts were analyzed after reaction for formation of carbonaceous deposits by C,H,N analysis. The 2CoDI was found to have 0.58 wt% carbon, and 2CoCA had 4.26 wt% carbon. This is initially an unexpected result since CA prepared catalysts showed higher activity and were stable longer. Similarly, Joo et al. found higher activity for catalysts that exhibited increased coke deposits in their study on nickel aluminates in methane dry reforming. It was suggested that amorphous carbon could cover all the active sites, whereas filamentous carbon could be grown not covering the metal surface, thus, allowing catalysts with higher amounts of coke to be more active. [64] Note that that 2CoDI deactivates faster relative to its original activity. It has been shown that certain types of carbonaceous species are required intermediates in the reaction between carbon dioxide and methane [8] and that the types of carbonaceous deposits are a function of metal particle size. [65-68] The extent of coke formation is a great indicator of the different types of active sites formed due to preparation method, CA or DI. [67, 69] The catalytic sites present on 2CoCA samples must propagate formation of non-deactivating coke deposits, while 2CoDI samples produce smaller amounts of deactivating coke deposits. Coke accumulation is the result of formation and gasification of carbonaceous deposits, thus the amount of carbon deposited depends on the relative rates of these processes. [43] The 2CoCA catalysts deactivate less quickly due to the large number of well-dispersed small particles. In other words, the formation of deactivating coke appears to be favored by the larger particles in 2CoDI. We speculate that the rapid deactivation observed for both samples (earlier for DI samples) is due to accelerated coke formation. The accelerated rate of deactivating by

carbonaceous deposits is believed to occur at a critical point where the ensemble size on the surface of the Co particles is too small to promote the carbon gasification reaction effectively. To confirm different types of carbonaceous deposits, post reaction catalysts were analyzed by XPS (Figure 9). The C1s spectrum was deconvoluted to reveal the types of carbonaceous species. [70]

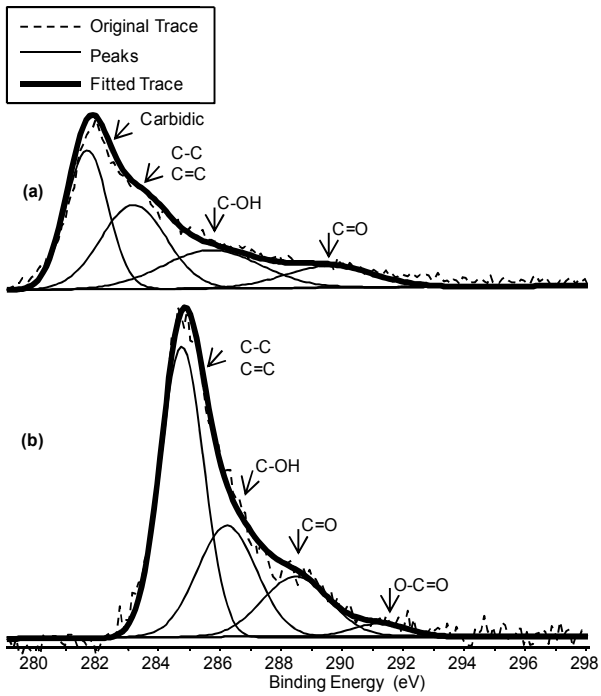

Figure 9 - X-ray photoelectron spectra in the C1s region of catalysts after 8 h methane dry reforming reaction (a) 2CoCA (b) 2CoDI.

For the 2CoCA sample a peak at 281.7 eV is attributed to the presence of carbidic carbon. Carbidic carbon has been shown to form on selective faces of cobalt particles. [71] The existence of carbidic carbon in the 2CoCA sample is attributed to the presence of nickel carbide phases that are commonly found on top of carbon filaments. Graphitic carbon can be clearly observed at 284.8 eV for 2CoDI. For 2CoCA graphitic carbon is attributed to the peak at 283.2 eV. Bulk cobalt carbide has been found to decompose to form graphitic carbon above 427 °C and is thought to cause the observed shift in binding energy for the 2CoCA. [71] In addition, peaks with higher binding energies were observed, which are attributed to oxidized carbon species. The

2CoCA sample contained carbidic, graphitic, and oxidic carbon in a ratio of 1:1:1, while the 2CoDI sample contained graphitic, and oxidic carbon in a ratio of 1:1. The formation of different types of carbonaceous deposits is attributed to the presence of different sites that resulted from the different preparation methods.

As can be seen from this work, monometallic cobalt catalysts have decent activity but suffer from deactivation due to coking under the conditions examined. Coke deposition was significant and likely the major cause of catalyst deactivation. As many studies have indicated, Ni-Co bimetallic catalysts could be very promising for carbon dioxide reforming of methane. [2, 43] In the case of Ni-Co bimetallics coke formation was found to be lower than in either monometallic Ni or Co. [43] Ni-Co bimetallics can also provide an H_2/CO greater than unity which is desirable for many industrial processes. It will be a promising approach to optimize metal particle size, composition, and uniformity of Ni-Co bimetallic catalysts for methane dry reforming using rational synthesis methods. By preparing these catalysts using rational synthesis methods, e.g. SEA/EDF well defined materials could be prepared which would aid in understanding of the coking mechanism that is likely causing catalyst deactivation in methane dry reforming.

Conclusions

Cobalt catalysts supported on γ-Al_2O_3 were prepared by two methods, controlled adsorption and dry impregnation. Deposition of Co^{2+} can be described by the kinetic equation suggested by Lycourghitis et al. indicating that two cobalt ions (presumably as a cobalt dimer) are involved in adsorption. [27] Controlling adsorption results in catalysts with smaller particle sizes and higher dispersion relative to the dry impregnation method studied. Adsorption of Co^{2+} on the Al_2O_3 surface likely involves mostly specific chemical interactions. Characterization results indicate

that the types of active sites present on a catalyst surface strongly depend on preparation method. TPR results indicated that 2CoCA catalysts were reduced to metallic Co to a greater extent than the 2CoDI samples. Additionally, more $CoAl_2O_4$ spinel type species were found to have formed for 2CoCA catalysts. Methane dry reforming studies indicate that cobalt alumina catalysts deactivate over the 8 h reaction time studied. However, 2CoCA catalysts show higher methane and carbon dioxide conversion, which is attributed to the higher dispersion of Co. The 2CoCA catalyst were found to produce higher amounts of non-deactivating coke deposits while the 2CoDI sample formed small amounts of deactivating coke deposits that drastically hindered catalyst activity and led to faster deactivation. The presence of two types of carbon deposition dependent on preparation method was confirmed by the use of XPS.

Acknowledgements

The authors wish to thank Micromeritics Corporation for TPR and H_2 chemisorption measurements. We also wish to thank Hye-Ran Cho, Jadid Samad, and John R. Regalbuto for valuable guidance on rational catalyst synthesis and for use of Matlab code. John R. Copeland and Sarah McNew are thanked for fruitful discussions. Funding from The Dow Chemical Company and the Institute of Paper Science is gratefully acknowledged.

References

1. D. Sutton, B. Kelleher and J. R. H. Ross, *Fuel Process. Technol.*, 2001, **73**, 155-173.
2. D. San-Jose-Alonso, J. Juan-Juan, M. J. Illan-Gomez and M. C. Roman-Martinez, *Appl. Catal. A: Gen.*, 2009, **371**, 54-59.
3. S. Y. Foo, C. K. Cheng, T. H. Nguyen and A. A. Adesina, *J. Mol. Catal. A: Chem.*, 2011, **344**, 28-36.
4. S. S. Pansare and J. D. Allison, *Appl. Catal. A: Gen.*, 2010, **387**, 224-230.
5. I. Chorkendorff, J. Niemantsverdriet, *Concepts of Modern Catalysis and Kinetics*, Wiely-VCH, 2011.
6. L. D'Souza, L. Jiao, J. R. Regalbuto, J. T. Miller and A. J. Kropf, *J. Catal.*, 2007, **248**, 165-174.
7. L. P. R. Profeti, E. A. Ticianelli and E. M. Assaf, *Fuel*, 2008, **87**, 2076-2081.
8. S. B. Wang, G. Q. M. Lu and G. J. Millar, *Energy Fuels*, 1996, **10**, 896-904.

9. J. Haber, J. H. Block and B. Delmon, *Pure Appl. Chem.*, 1995, **67**, 1257-1306.
10. K. P. d. Jong, *Synthesis of Solid Catalysts*, Wiley, Utrecht, 2009.
11. T. Ataloglou, J. Vakros, K. Bourikas, C. Fountzoula, C. Kordulis and A. Lycourghiotis, *Appl. Catal. B: Environ.*, 2005, **57**, 299-312.
12. J. R. Regalbuto, in *Catalyst Preparation*, CRC Press, 2006, pp. 297-318.
13. M. Neurock, *J. Catal.*, 2003, **216**, 73-88.
14. J. R. Regalbuto, A. Navada, S. Shadid, M. L. Bricker and Q. Chen, *J. Catal.*, 1999, **184**, 335-348.
15. M. Schreier and J. R. Regalbuto, *J. Catal.*, 2004, **225**, 190-202.
16. J. T. Miller, M. Schreier, A. J. Kropf and J. R. Regalbuto, *J. Catal.*, 2004, **225**, 203-212.
17. L. Jiao and J. R. Regalbuto, *J. Catal.*, 2008, **260**, 329-341.
18. L. Jiao and J. R. Regalbuto, *J. Catal.*, 2008, **260**, 342-350.
19. X. Hao, L. Quach, J. Korah, W. A. Spieker and J. R. Regalbuto, *J. Mol. Catal. A: Chem.*, 2004, **219**, 97-107.
20. J. Korah, W. A. Spieker and J. R. Regalbuto, *Catal. Lett.*, 2003, **85**, 123-127.
21. L. Jiao, Y. Zha, X. Hao and J. R. Regalbuto, in *Scientific Bases for the Preparation of Heterogeneous Catalysts, Proceedings of the 9th International Symposium*, eds. E. M. Gaigneaux, M. Devillers, D. E. De Vos, S. Hermans, P. A. Jacobs, J. A. Martens and P. Ruiz, 2006, vol. 162, pp. 211-218.
22. L. Vordonis, N. Spanos, P. G. Koutsoukos and A. Lycourghiotis, *Langmuir*, 1992, **8**, 1736-1743.
23. N. Spanos and A. Lycourghiotis, *J. Chem. Soc. Faraday Trans.*, 1993, **89**, 4101-4107.
24. J. Vakros, K. Bourikas, S. Perlepes, C. Kordulis and A. Lycourghiotis, *Langmuir*, 2004, **20**, 10542-10550.
25. K. Bourikas, C. Kordulis, J. Vakros and A. Lycourghiotis, *Adv. Colloid Interface Sci.*, 2004, **110**, 97-120.
26. T. Ataloglou, K. Bourikas, J. Vakros, C. Kordulis and A. Lycourghiotis, *J. Phys. Chem. B*, 2005, **109**, 4599-4607.
27. K. Bourikas, C. Kordulis and A. Lycourghiotis, *Catal. Rev.: Sci. Eng.*, 2006, **48**, 363-444.
28. K. Bourikas, J. Vakros, C. Fountzoula, C. Kordulis and A. Lycourghiotis, *Catal. Today*, 2007, **128**, 138-144.
29. X. Hao, W. A. Spieker and J. R. Regalbuto, *J. Colloid Interface Sci.*, 2003, **267**, 259-264.
30. D. W. Fuerstenau and K. Osseoasare, *J. Colloid Interface Sci.*, 1987, **118**, 524-542.
31. P. H. Tewari and W. Lee, *J. Colloid Interface Sci.*, 1975, **52**, 77-88.
32. R. O. James and T. W. Healy, *J. Colloid Interface Sci.*, 1972, **40**, 65-81.
33. P. K. Debokx, W. B. A. Wassenberg and J. W. Geus, *J. Catal.*, 1987, **104**, 86-98.
34. A. Haworth, *Adv. Colloid Interface Sci.*, 1990, **32**, 43-78.
35. C. H. Bartholomew and R. J. Farrauto, *J. Catal.*, 1976, **45**, 41-53.
36. K. B. Agashe and J. R. Regalbuto, *J. Colloid Interface Sci.*, 1997, **185**, 174-189.
37. J. A. Schwarz, Contescu, C., *Surfaces of Nanoparticles And Porous Materials*, Ipswich, MA, 1999.
38. W. G. Schlaffer, C. Z. Morgan and J. N. Wilson, *J. Phys. Chem*, 1957, **61**, 714-722.
39. Holleman-Wiberg, *Inorganic Chemistry*, Academic Press, 2001.
40. W. Stumm, H. Hohl and F. Dalang, *Croat. Chem. Acta*, 1976, **48**, 491-504.
41. E. Ruckenstein and H. Y. Wang, *J. Catal.*, 2002, **205**, 289-293.
42. S. A. Hosseini, A. Taeb and F. Feyzi, *Catal. Commun.*, 2005, **6**, 233-240.
43. J. G. Zhang, H. Wang and A. K. Dalai, *J. Catal.*, 2007, **249**, 300-310.
44. B. Jongsomjit, J. Panpranot and J. G. Goodwin, *J. Catal.*, 2001, **204**, 98-109.
45. N. Job, S. Lambert, M. Chatenet, C. J. Gommes, F. Maillard, S. Berthon-Fabry, J. R. Regalbuto and J.-P. Pirard, *Catal. Today*, 2010, **150**, 119-127.
46. B. Scheffer, P. Molhoek and J. A. Moulijn, *Appl. Catal.*, 1989, **46**, 11-30.

47. J. M. Rynkowski, T. Paryjczak and M. Lenik, *Appl. Catal. A: Gen.*, 1993, **106**, 73-82.
48. Y.-W. C. Hsin-Yu Lin, *Mater. Chem. Phys.*, 2003, 171-175.
49. R. Bechara, D. Balloy, J. Y. Dauphin and J. Grimblot, *Chem. Mater.*, 1999, **11**, 1703-1711.
50. L. Guczi, T. Hoffer, Z. Zsoldos, S. Zyade, G. Maire and F. Garin, *J. Phys. Chem*, 1991, **95**, 802-808.
51. Z. Zsoldos and L. Guczi, *J. Phys. Chem*, 1992, **96**, 9393-9400.
52. W. J. Wang and Y. W. Chen, *Appl. Catal.*, 1991, **77**, 223-233.
53. P. Arnoldy and J. A. Moulijn, *J. Catal.*, 1985, **93**, 38-54.
54. J. Y. Yan, M. C. Kung, W. M. H. Sachtler and H. H. Kung, *J. Catal.*, 1997, **172**, 178-186.
55. Y. J. Lee, J. Y. Park, K. W. Jun, J. W. Bae and P. S. S. Prasad, *Catal. Lett.*, 2009, **130**, 198-203.
56. P. H. Bolt, F. Habraken and J. W. Geus, *J. Solid State Chem.*, 1998, **135**, 59-69.
57. R. Bouarab, O. Cherifi and A. Auroux, *Green Chem.*, 2003, **5**, 209-212.
58. D. S. Jose-Alonso, M. J. Illan-Gomez and M. C. Roman-Martinez, *Int. J. Hydrogen Energy*, 2013, **38**, 2230-2239.
59. E. Ruckenstein and H. Y. Wang, *Appl. Catal. A: Gen.*, 2000, **204**, 257-263.
60. P. Ferreira-Aparicio, A. Guerrero-Ruiz and I. Rodriguez-Ramos, *Appl. Catal. A: Gen.*, 1998, **170**, 177-187.
61. A. W. Budiman, S.-H. Song, T.-S. Chang, C.-H. Shin and M.-J. Choi, *Catal. Surv. Asia*, 2012, **16**, 183-197.
62. K. Takanabe, K. Nagaoka, K. Nariai and K. Aika, *J. Catal.*, 2005, **230**, 75-85.
63. J. van de Loosdrecht, B. Bazhinimaev, J. A. Dalmon, J. W. Niemantsverdriet, S. V. Tsybulya, A. M. Saib, P. J. van Berge and J. L. Visagie, *Catal. Today*, 2007, **123**, 293-302.
64. O. S. Joo and K. D. Jung, *Bull. Korean Chem. Soc.*, 2002, **23**, 1149-1153.
65. J. R. Rostrup-Nielsen, *J. Catal.*, 1972, **27**, 343-356.
66. N. Sahli, C. Petit, A. C. Roger, A. Kiennemann, S. Libs and M. M. Bettahar, *Catal. Today*, 2006, **113**, 187-193.
67. R. T. K. Baker, *Carbon*, 1989, **27**, 315-323.
68. R. T. K. Baker, P. S. Harris, R. B. Thomas and R. J. Waite, *J. Catal.*, 1973, **30**, 86-95.
69. J. R. Rostrup-Nielsen, *J. Catal.*, 1984, **85**, 31-43.
70. J. W. Long, M. Laskoski, G. W. Peterson, T. M. Keller, K. A. Pettigrew and B. J. Schindler, *J. Mater. Chem.*, 2011, **21**, 3477-3484.
71. J. Nakamura, I. Toyoshima and K. Tanaka, *Surf. Sci.*, 1988, **201**, 185-194.

Cobalt alumina catalysts were synthesized by dry impregnation and controlled adsorption. The effect of catalyst preparation method was studied on methane steam reforming.